



# Mixed 3d/4d and 3d/4f metal clusters: Tetranuclear $\text{Fe}_2^{\text{III}}\text{M}_2^{\text{III}}$ ( $\text{M}^{\text{III}} = \text{Ln}, \text{Y}$ ) and $\text{Mn}_2^{\text{IV}}\text{M}_2^{\text{III}}$ ( $\text{M} = \text{Yb}, \text{Y}$ ) complexes, and the first Fe/4f single-molecule magnets

Muralee Murugesu<sup>a</sup>, Abhudaya Mishra<sup>a</sup>, Wolfgang Wernsdorfer<sup>b</sup>,  
Khalil A. Abboud<sup>a</sup>, George Christou<sup>a,\*</sup>

<sup>a</sup> Department of Chemistry, University of Florida, Gainesville, FL 32611-7200, USA

<sup>b</sup> Laboratoire Louis Néel-CNRS, BP 166, 25 Avenue des Martyrs, 38042 Grenoble, Cedex 9, France

Received 6 July 2005; accepted 18 August 2005

Available online 21 November 2005

Dedicated to Malcolm H. Chisholm on the occasion of his 60th birthday; an outstanding scientist, colleague, and friend.

## Abstract

The synthesis, structure and magnetic properties are reported of  $\text{Fe}_2\text{Ln}_2$ ,  $\text{Fe}_2\text{Y}_2$ ,  $\text{Mn}_2\text{Yb}_2$  and  $\text{Mn}_2\text{Y}_2$  complexes. The compound  $[\text{Fe}_2\text{Ho}_2(\text{OH})_2(\text{teaH})_2(\text{O}_2\text{CPh})_4(\text{NO}_3)_2]$  (**1**), where teaH<sub>3</sub> is triethanolamine, was obtained from the reaction of eight equivalents of teaH<sub>3</sub> with one equivalent each of  $\text{Ho}(\text{NO}_3)_3$  and  $[\text{Fe}_3\text{O}(\text{O}_2\text{CPh})_6(\text{H}_2\text{O})_3](\text{O}_2\text{CPh})$  in MeCN/MeOH. The use instead of  $\text{Dy}(\text{NO}_3)_3$  or  $\text{Tb}(\text{NO}_3)_3$  leads to the structurally similar products  $[\text{Fe}_2\text{Dy}_2(\text{OH})_2(\text{teaH})_2(\text{O}_2\text{CPh})_6]$  (**2**) and  $[\text{Fe}_2\text{Tb}_2(\text{OH})_2(\text{teaH})_2(\text{O}_2\text{CPh})_6]$  (**3**). The compounds  $[\text{Fe}_2\text{Y}_2(\text{pdmH})_6\text{Cl}_4]\text{Cl}_2$  (**4**) and isostructural  $[\text{Fe}_2\text{Ho}_2(\text{pdmH})_6\text{Cl}_4]\text{Cl}_2$  (**5**), where pdmH<sub>2</sub> is pyridine-2,6-dimethanol, were prepared from the reaction of four equivalents of pdmH<sub>2</sub> with two equivalents of  $\text{YCl}_3$  or  $\text{HoCl}_3$ , respectively, and  $\text{FeCl}_2$  in MeOH. The compounds  $[\text{Mn}_2\text{Y}_2\text{O}_2(\text{O}_2\text{CPh})_6(\text{OMe})_4(\text{MeOH})_4]$  (**6**) and  $[\text{Mn}_2\text{Yb}_2\text{O}_2(\text{O}_2\text{CPh})_6(\text{OMe})_4(\text{MeOH})_4]$  (**7**) were prepared by methanolysis of  $(\text{NBu}_4)^+[\text{Mn}_4\text{O}_2(\text{O}_2\text{CPh})_9(\text{H}_2\text{O})]$  in the presence of  $\text{Yb}(\text{NO}_3)_3$  or  $\text{Y}(\text{NO}_3)_3$ , respectively. Complexes **1–3**, **6** and **7** contain a ‘defect cubane’  $\text{M}_4$  core (including the first mixed 3d/4f examples of this type to contain  $\text{Fe}^{\text{III}}$  or  $\text{Mn}^{\text{IV}}$ ), whereas **4** and **5** have a U-shaped core. Variable-temperature solid-state magnetic susceptibility studies of **1–6** in the temperature range 5.00–300 K were carried out, and for all the complexes predominantly antiferromagnetic exchange interactions between the metal centers was observed. Magnetization versus applied field sweeps on single crystals of **1** and **2** at low temperature reveal hysteresis loops, confirming these species to be new examples of single-molecule magnets (SMMs). Thus, complexes **1** and **2** are the first examples of Fe/4f SMMs.

© 2005 Elsevier Ltd. All rights reserved.

**Keywords:** Iron; Manganese; Lanthanide; Single-molecule magnet; Crystal structures; Hysteresis

## 1. Introduction

A major reason for the current intense interest by many groups around the world in polynuclear 3d transition metal clusters is the often unusual and even novel magnetic properties such species possess. In particular, some of these

clusters have been found to be single-molecule magnets (SMMs), which are individual molecules capable of functioning as nanoscale magnetic particles and which thus represent a molecular approach to nanomagnetism [1–3]. In addition, there continues to be a great bioinorganic chemistry interest in 3d metal clusters, which are of relevance to objectives such as understanding the assembly of the multinuclear Fe/O core of the iron-storage protein ferritin, and elucidating the nature and mechanism of action of the  $\text{Mn}_4\text{Ca}$  core of the water oxidizing complex of

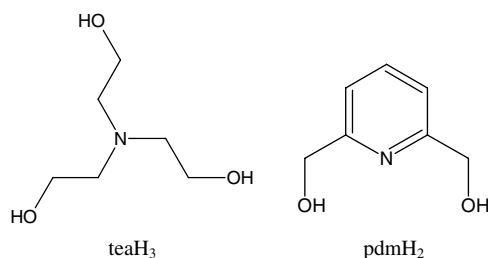
\* Corresponding author.

E-mail addresses: [christou@chem.ufl.edu](mailto:christou@chem.ufl.edu), [polyhedron@chem.ufl.edu](mailto:polyhedron@chem.ufl.edu) (G. Christou).

photosystem II [4–8]. For these and other areas, there continues to be a great need for synthetic methods to new examples of homometallic and heterometallic metal clusters, to increase our knowledge of the structural, magnetic, and other properties of high nuclearity paramagnetic species.

The present paper reports results of relevance to the nanomagnetism field. SMMs, which are molecular superparamagnets, derive their properties from the combination of a large ground state spin ( $S$ ) value and a large and negative magnetoanisotropy (negative zero-field splitting parameter,  $D$ ). This combination results in a significant energy barrier to magnetization reversal, and hence slow relaxation of the magnetization is observed at low temperatures. The latter can be detected as: (i) frequency-dependent signals in AC susceptibility measurements; (ii) hysteresis in magnetization versus applied DC field sweeps [1–3,9–12]. There are now many homometallic SMMs, most of them Mn species [13], and new approaches into heterometallic species have been more recently explored as a route to distinctly different properties. As a result of such work, we and others have recently reported some mixed transition metal/lanthanide SMMs [14–16]. In this paper, we report the extension of our studies along these lines and describe new Fe/Ln and Mn/Ln clusters. Not all of these are new SMMs, but they are all nevertheless valuable new additions to the growing family of mixed 3d/4f clusters possessing a variety of structural and other properties. We also have extended this work to Y instead of Ln, which has proven useful for understanding the magnetic properties of the isostructural Ln-containing species.

To facilitate the formation of polynuclear products, this work has employed the polydentate chelate-forming molecules triethanolamine ( $\text{teaH}_3$ ) and pyridine-2,6-dimethanol ( $\text{pdmH}_2$ ). Both molecules contain alcohol arms, which are good metal-bridging groups on deprotonation and thus foster formation of polynuclear products [17–20]. In addition, since lanthanides show strong affinity towards oxygen donors [23], both chelates were thought likely to lead to mixed 3d/4f products, and this has proven to be the case. We herein report the synthesis, crystallographic characterization and magnetic properties of a family of mixed 3d/4f M/Ln ( $M = \text{Mn}, \text{Fe}$ ) and mixed M/Y ( $M = \text{Mn}, \text{Fe}$ ) complexes. These are also the first crystallographically characterized tetranuclear  $\text{Fe}^{\text{III}}/\text{Ho}^{\text{III}}$ ,  $\text{Fe}^{\text{III}}/\text{Y}^{\text{III}}$ ,  $\text{Mn}^{\text{IV}}/\text{Yb}^{\text{III}}$  and  $\text{Mn}^{\text{IV}}/\text{Y}^{\text{III}}$  complexes in general.



## 2. Experimental

### 2.1. Compound preparations

All manipulations were performed under aerobic conditions using materials and solvents as received.  $[\text{Fe}_3\text{O}(\text{O}_2\text{CR})_6(\text{H}_2\text{O})_3](\text{O}_2\text{CR})$  and  $(\text{NBu}_4^+)[\text{Mn}_4\text{O}_2(\text{O}_2\text{CPh})_9(\text{H}_2\text{O})]$  complexes were prepared using the procedures reported previously [24,25].

#### 2.1.1. $[\text{Fe}_2\text{Ho}_2(\text{OH})_2(\text{teaH})_2(\text{O}_2\text{CPh})_4(\text{NO}_3)_2] \cdot 6\text{MeCN}$ (**1** · 6MeCN)

Solutions of  $[\text{Fe}_3\text{O}(\text{O}_2\text{CPh})_6(\text{H}_2\text{O})_3](\text{O}_2\text{CPh})$  (0.26 g, 0.25 mmol) in MeCN (30 mL), and  $\text{Ho}(\text{NO}_3)_3 \cdot 5\text{H}_2\text{O}$  (0.11 g, 0.25 mmol) and  $\text{teaH}_3$  (0.298 g, 2 mmol) in MeCN/MeOH (50/5 mL) were mixed to give a yellow/orange solution. This was layered with  $\text{Et}_2\text{O}$  and left undisturbed at room temperature. After 7 days, small yellow rectangular crystals of **1** · 6MeCN were collected in 40% yield and dried in vacuum. *Anal. Calc.* for **1**: C, 34.85; H, 3.51; N, 4.06. Found: C, 34.99; H, 3.54; N, 4.38%. Selected IR data ( $\text{cm}^{-1}$ ): 3510 (br), 2860 (s), 1595 (s), 1541 (m), 1381 (m), 1095 (s), 909 (s), 723 (m), 674 (m), 595 (s), 460 (s).

#### 2.1.2. $[\text{Fe}_2\text{Dy}_2(\text{OH})_2(\text{teaH})_2(\text{O}_2\text{CPh})_6] \cdot 4\text{MeCN} \cdot 3\text{H}_2\text{O}$ (**2** · 4MeCN · 3H<sub>2</sub>O)

This was prepared in a similar way as **1**, but using  $\text{Dy}(\text{NO}_3)_3 \cdot 6\text{H}_2\text{O}$  instead of  $\text{Ho}(\text{NO}_3)_3 \cdot 5\text{H}_2\text{O}$ . After 2 days, pale yellow rectangular crystals of **2** · 4MeCN · 3H<sub>2</sub>O were collected in 52% yield and dried in air. *Anal. Calc.* for **2** · 4MeCN · 3H<sub>2</sub>O: C, 43.55; H, 4.47; N, 4.91. Found: C, 43.48; H, 4.20; N, 4.90%. Selected IR data ( $\text{cm}^{-1}$ ): 3420 (br), 2860 (m), 1595 (s), 1544 (m), 1448 (m), 1095 (m), 1025 (s), 907 (s), 721 (m), 674 (s), 594 (s), 460 (s).

#### 2.1.3. $[\text{Fe}_2\text{Tb}_2(\text{OH})_2(\text{teaH})_2(\text{O}_2\text{CPh})_6] \cdot 4\text{MeCN} \cdot 3\text{H}_2\text{O}$ (**3** · 4MeCN · 3H<sub>2</sub>O)

This was prepared in a similar way as **1**, but using  $\text{Tb}(\text{NO}_3)_3 \cdot 6\text{H}_2\text{O}$  instead of  $\text{Ho}(\text{NO}_3)_3 \cdot 5\text{H}_2\text{O}$ . After 2 days, pale yellow rectangular crystals of **3** · 4MeCN · 3H<sub>2</sub>O were collected in 49% yield and dried in air. *Anal. Calc.* for **3** · 4MeCN · 3H<sub>2</sub>O: C, 43.73; H, 4.49; N, 4.93. Found: C, 43.66; H, 4.15; N, 4.86%. Selected IR data ( $\text{cm}^{-1}$ ): 3380 (br), 2860 (m), 1595 (s), 1545 (m), 1448 (m), 1094 (m), 1025 (s), 905 (s), 718 (m), 674 (s), 593 (s), 459 (s).

#### 2.1.4. $[\text{Fe}_2\text{Y}_2(\text{pdmH})_6\text{Cl}_4]\text{Cl}_2 \cdot 2\text{MeOH}$ (**4** · 2MeOH)

Solutions of  $\text{FeCl}_2 \cdot 4\text{H}_2\text{O}$  (0.10 g, 0.50 mmol) in MeOH (20 mL), and  $\text{YCl}_3 \cdot 6\text{H}_2\text{O}$  (0.15 g, 0.50 mmol) and  $\text{pdmH}_2$  (0.14 g, 1.0 mmol) in MeOH (20 mL) were mixed to give a yellow solution. This was layered with  $\text{Et}_2\text{O}$  and left undisturbed at room temperature. After 7 days, small yellow rectangular crystals of **4** · 2MeOH were collected in 42% yield and dried in vacuum. *Anal. Calc.* for **4**: C, 37.87; H,

4.05; N, 6.02. Found: C, 37.51; H, 3.93; N, 5.87%. Selected IR data ( $\text{cm}^{-1}$ ): 3376 (br), 3075 (br), 1607 (m), 1579 (s), 1447 (m), 1368 (s), 1360 (s), 1163 (s), 1072 (m), 1046 (m), 783 (m), 654 (s), 554 (s), 497 (s).

#### 2.1.5. $[\text{Fe}_2\text{Ho}_2(\text{pdmH})_6\text{Cl}_4]\text{Cl}_2 \cdot 2\text{MeOH} (5 \cdot 2\text{MeOH})$

Solutions of  $\text{FeCl}_2 \cdot 4\text{H}_2\text{O}$  (0.10 g, 0.50 mmol) in MeOH (20 mL), and  $\text{HoCl}_3 \cdot 6\text{H}_2\text{O}$  (0.19 g, 0.50 mmol) and  $\text{pdmH}_2$  (0.14 g, 1.0 mmol) in MeOH (20 mL) were mixed to give a yellow/green solution. This was layered with  $\text{Et}_2\text{O}$  and left undisturbed at room temperature. After 7 days, small yellow/green rectangular crystals of **5** were collected in 37% yield and dried in vacuum. *Anal. Calc.* for **5**: C, 34.15; H, 3.65; N, 5.43. Found: C, 34.23; H, 3.54; N, 5.26%. Selected IR data ( $\text{cm}^{-1}$ ): 3437 (br), 3317 (br), 3007 (br), 2834 (br), 2713 (br), 2621 (br), 1609 (m), 1582 (s), 1448 (m), 1310 (m), 1042 (m), 797 (s), 725 (s), 667(s), 576(s), 475(s).

#### 2.1.6. $[\text{Mn}_2\text{Y}_2\text{O}_2(\text{O}_2\text{CPh})_6(\text{OMe})_4(\text{MeOH})_4] \cdot 2\text{MeOH} (6 \cdot 2\text{MeOH})$

$(\text{NBu}_4^n)[\text{Mn}_4\text{O}_2(\text{O}_2\text{CPh})_9(\text{H}_2\text{O})]$  (0.50 g, 1.0 mmol) was dissolved in a solution of  $\text{Y}(\text{NO}_3)_3 \cdot 6\text{H}_2\text{O}$  (0.24 g, 2.0 mmol) in MeCN/MeOH (20/5 mL) and stirred for 25 min to give a brown solution. This was filtered and more MeOH (10 mL) added to the filtrate. The resulting solution was left undisturbed at room temperature for a week to slowly produce orange crystals of **6**  $\cdot 2\text{MeOH}$ , which were collected in 25% yield and dried in vacuum. The same product was obtained using  $\text{YCl}_3 \cdot 6\text{H}_2\text{O}$  instead of  $\text{Y}(\text{NO}_3)_3 \cdot 6\text{H}_2\text{O}$ . *Anal. Calc.* for **6**: C, 46.24; H, 4.50. Found: C, 46.15; H, 4.46%. Selected IR data ( $\text{cm}^{-1}$ ): 3412 (br), 1594 (m), 1545 (s), 1448 (w), 1391 (s), 1025 (w), 718 (s), 681 (m), 623 (s), 540 (m), 474 (w).

#### 2.1.7. $[\text{Mn}_2\text{Yb}_2\text{O}_2(\text{O}_2\text{CPh})_6(\text{OMe})_4(\text{MeOH})_4] \cdot 2\text{MeOH} (7 \cdot 2\text{MeOH})$

$(\text{NBu}_4^n)[\text{Mn}_4\text{O}_2(\text{O}_2\text{CPh})_9(\text{H}_2\text{O})]$  (0.50 g, 1.0 mmol) was dissolved in a solution of  $\text{Yb}(\text{NO}_3)_3 \cdot 5\text{H}_2\text{O}$  (0.31 g, 2.0 mmol) in MeCN/MeOH (20/5 mL) and stirred for 25 min to give a brown solution. This was filtered and more MeOH (10 mL) added to the filtrate. The resulting solution was slowly concentrated by evaporation at room temperature for 5 days, during which time brown crystals of **7**  $\cdot 2\text{MeOH}$  slowly grew. These were collected in 10% yield and dried in vacuum. *Anal. Calc.* for **7**: C, 40.94; H, 3.99. Found: C, 40.87; H, 3.96%. Selected IR data ( $\text{cm}^{-1}$ ): 3426 (br), 1600 (m), 1540 (m), 1384 (s), 1026 (w), 718 (s), 682 (m), 624 (s), 545 (m), 476 (w).

## 2.2. General and physical measurements

Elemental analyses (C, H and N) were performed in the in-house facilities of the University of Florida Chemistry Department. Infrared spectra in the 400–4000  $\text{cm}^{-1}$  range were recorded in the solid state (KBr pellets) on a Nicolet Nexus 670 FTIR spectrometer. Variable temperature DC magnetic susceptibility data down to 5.0 K were collected using a Quantum Design MPMS-XL SQUID susceptometer equipped with a 7 T DC magnet. Pascal's constants were used to estimate the diamagnetic corrections, which were subtracted from the experimental susceptibilities to give the molar magnetic susceptibilities ( $\chi_M$ ). Microcrystalline samples were restrained in eicosane by suspending the solid for 15 min in eicosane maintained at a temperature above its melting point (35–37 °C), and then the temperature was gradually decreased below the melting point to solidify the eicosane. Low-temperature (<1.8 K) hysteresis loop and DC relaxation measurements were performed at Grenoble using an array of micro-SQUIDs [26].

Table 1  
Crystallographic data for complexes **1**, **4**, **5**, **6** and **7**

Compound	<b>1</b>	<b>4</b>	<b>5</b>	<b>6</b>	<b>7</b>
Formula	$\text{C}_{52}\text{H}_{66}\text{Fe}_2\text{Ho}_2\text{N}_{10}\text{O}_{22}$	$\text{C}_{46}\text{H}_{64}\text{Cl}_6\text{Fe}_2\text{N}_6\text{O}_{16}\text{Y}_2$	$\text{C}_{46}\text{H}_{64}\text{Cl}_6\text{Fe}_2\text{N}_6\text{O}_{16}\text{Ho}_2$	$\text{C}_{52}\text{H}_{66}\text{Mn}_2\text{O}_{24}\text{Y}_2$	$\text{C}_{52}\text{H}_{66}\text{Mn}_2\text{O}_{24}\text{Yb}_2$
Formula weight	1624.17	1459.25	1611.29	1362.75	1531.01
Space group	$P\bar{1}$	$I2/a$	$I2/a$	$P2_1/c$	$P2_1/c$
<i>a</i> (Å)	12.0151(8)	20.9871(15)	20.9871(15)	15.6620(12)	15.5610(11)
<i>b</i> (Å)	12.1189(8)	19.1467(14)	19.1467(14)	24.9417(19)	24.9105(18)
<i>c</i> (Å)	12.8580(8)	14.6204(11)	14.6204(11)	7.8231(6)	7.8259(6)
$\alpha$ (°)	116.348(2)	90	90	90	90
$\beta$ (°)	94.752(2)	92.745(2)	92.7450(10)	95.819(2)	96.120(2)
$\gamma$ (°)	103.419(2)	90	90	90	90
<i>V</i> (Å <sup>3</sup> )	1594.42(18)	5868.2(7)	5868.2(7)	3040.2(4)	3016.3(4)
<i>Z</i>	1	4	4	2	2
<i>T</i> (°C)	173(2)	173(2)	173(2)	173(2)	173(2)
Radiation	Mo K $\alpha$	Mo K $\alpha$	Mo K $\alpha$	Mo K $\alpha$	Mo K $\alpha$
$\rho_{\text{calc}}$ (g/cm <sup>-3</sup> )	1.692	1.652	1.824	1.489	1.686
$\mu$ (mm <sup>-1</sup> )	2.981	2.785	3.494	2.372	3.558
$R_1^{\text{a,b}}$	3.55	4.02	3.59	3.48	3.11
$wR_2^{\text{a,c}}$	8.62	9.94	9.62	7.27	7.67

<sup>a</sup>  $I > 2\sigma(I)$ .

<sup>b</sup>  $R_1 = 100 \sum (||F_o| - |F_c||) / \sum |F_o|$ .

<sup>c</sup>  $wR_2 = 100 \sum [w(F_o^2 - F_c^2)^2]^{1/2} / \sum [w(F_o^2)^2]^{1/2}$ ,  $w = 1/[\sigma^2(F_o^2) + (ap)^2 + bp]$ , where  $p = [\max(F_o^2, 0) + 2F_c^2]/3$ .

### 2.2.1. X-ray crystallography and solution of structures

Data were collected at 173 K on a Siemens SMART PLATFORM equipped with a CCD area detector and a graphite monochromator utilizing Mo K $\alpha$  radiation ( $\lambda = 0.71073$  Å). Cell parameters were refined using up to 8192 reflections. A full sphere of data (1850 frames) was collected using the  $\omega$ -scan method ( $0.3^\circ$  frame width). The first 50 frames were re-measured at the end of data collection to monitor instrument and crystal stability (maximum correction on  $I$  was  $<1\%$ ). Absorption corrections by integration were applied based on measured indexed crystal faces.

The structures were solved by the direct methods in SHELXL6 [27], and refined using full-matrix least squares. The non-hydrogen atoms were refined anisotropically, whereas the hydrogen atoms were placed in ideal,

calculated positions and refined isotropically as riding on their respective carbon atoms. For complex **1**·6MeCN, a total of 405 parameters were refined in the final cycle of refinement using 5899 reflections with  $I > 2\sigma(I)$ . For complex **4**·2MeOH, a total of 365 parameters were refined in the final cycle of refinement using 4504 reflections with  $I > 2\sigma(I)$ . For complex **5**·2MeOH, a total of 365 parameters were refined in the final cycle of refinement using 4670 reflections with  $I > 2\sigma(I)$ . For complex **6**·2MeOH, a total of 378 parameters were refined in the final cycle of refinement using 2803 reflections with  $I > 2\sigma(I)$ . For complex **7**·2MeOH, a total of 378 parameters were refined in the final cycle of refinement on  $F^2$  using 4821 reflections with  $I > 2\sigma(I)$ . Unit cell data and the final refinement indices  $R_1$  and  $wR_2$  are listed in Table 1.

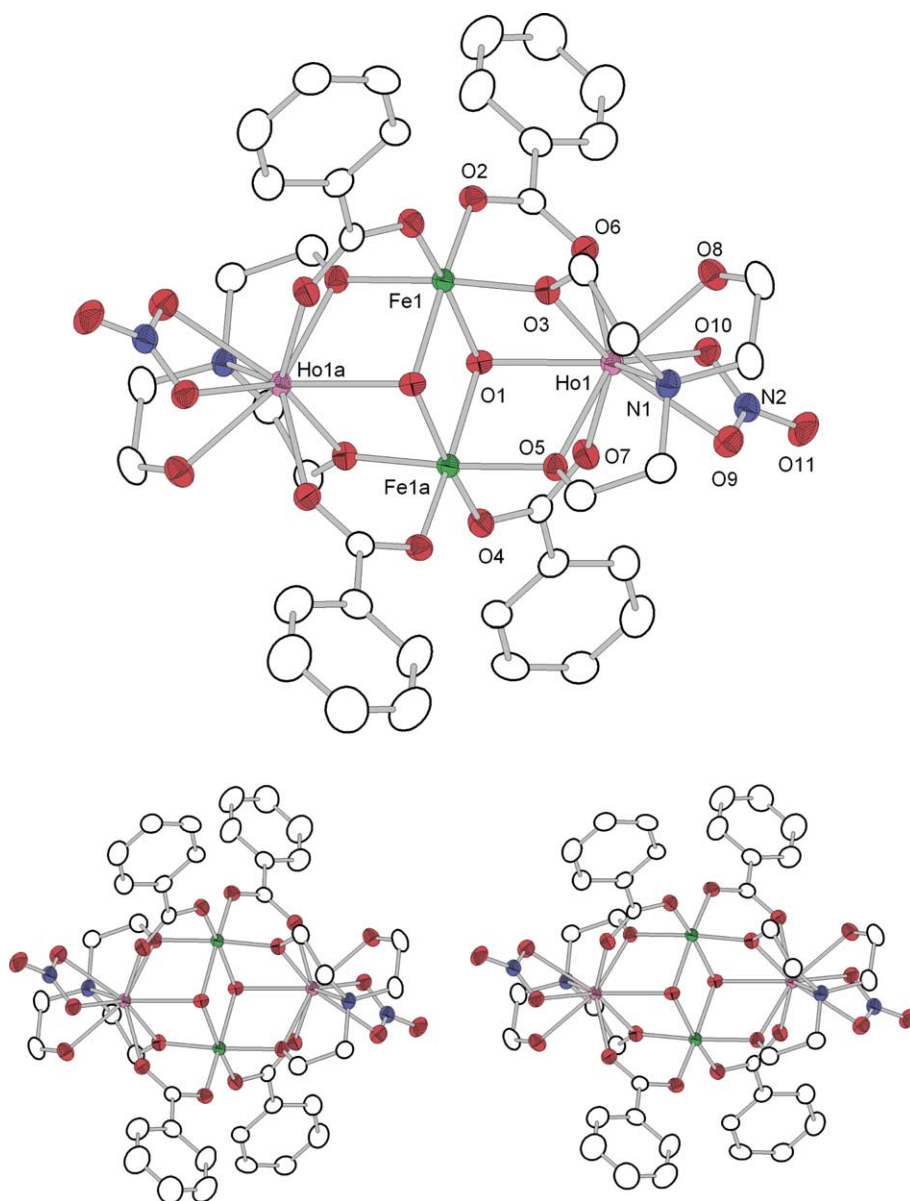


Fig. 1. ORTEP representation and stereopair at the 50% probability level of complex **1**. All H atoms have been removed for clarity.

### 3. Results and discussion

#### 3.1. Syntheses

The reaction of a  $[M_3O(O_2CR)_6L_3]^{0,+}$  ( $M = Mn, Fe$ ;  $L = py, H_2O$ , etc.) complex with a chelating ligand represents a commonly employed and successful route to a wide range of higher nuclearity clusters of Fe and Mn. For example, the use of triethanolamine (teaH<sub>3</sub>) or 2-(hydroxymethyl)pyridine (hmpH) has led to a large variety of products, depending on the precise reaction conditions and ratios, including Mn<sub>4</sub> [28], Mn<sub>6</sub> [21], Fe<sub>8</sub> [22], Mn<sub>7</sub> [29], Mn<sub>10</sub> [30], Mn<sub>12</sub> [31], and Fe<sub>6</sub> [32] clusters. As stated earlier, the alkoxide arms of the tea<sup>3-</sup> and hmp<sup>-</sup> ligands normally adopt bridging modes, fostering formation of higher nuclearity products. Thus, we have employed  $[Fe_3O(O_2CPh)_6(H_2O)_3]^+$  or FeCl<sub>2</sub> and a lanthanide Ln<sup>3+</sup> (or Y<sup>3+</sup>) source in reactions with teaH<sub>3</sub> or pdmH<sub>2</sub> in MeOH or a mixed MeOH/MeCN solvent system (to ensure adequate solubility of all reagents).

The reaction of  $[Fe_3O(O_2CPh)_6(H_2O)_3](O_2CR)$ , Ln(NO<sub>3</sub>)<sub>3</sub> (Ln = Ho, Dy, Tb) and teaH<sub>3</sub> in a 1:1:8 molar ratio in MeCN/MeOH gave yellow solutions from which yellow rectangular crystals of  $[Fe_2Ho_2(OH)_2(teaH)_2(O_2CPh)_4(NO_3)_2]$  (**1**),  $[Fe_2Dy_2(OH)_2(teaH)_2(O_2CPh)_6]$  (**2**) and  $[Fe_2Tb_2(OH)_2(teaH)_2(O_2CPh)_6]$  (**3**) slowly formed in ~40–50% yields. If the reaction solutions were left undisturbed for longer periods (~2 weeks), orange crystals of the known homometallic complex  $[Fe_8O_3(O_2CPh)_9(tea)(teaH)_3]$  were also obtained [22]. The reactions are likely complicated equilibria involving several species of various nuclearities, both homo- and heterometallic, and the crystallization of the main product directly from the reaction solution is probably beneficial in providing pure material. In all cases, the filtrates are still colored, but we have not pursued isolation of other species (other than  $[Fe_8O_3(O_2CPh)_9(tea)(teaH)_3]$ ).

Treatment of an equimolar mixture of FeCl<sub>2</sub> and YCl<sub>3</sub> in MeOH with two equivalents of pdmH<sub>2</sub> gave a yellow solution, and layering this with Et<sub>2</sub>O gave small rectangular yellow crystals of  $[Fe_2Y_2(pdmH)_6Cl_4]Cl_2$  (**4**) in 42% yield. The same reaction but with HoCl<sub>3</sub> gave the analogous  $[Fe_2Ho_2(pdmH)_6Cl_4]Cl_2$  (**5**) complex in 37% yield. Small changes to the Fe:Ln:pdmH<sub>2</sub> ratio still gave the same products.

A different strategy was used for the Mn reactions. In this case, neither teaH<sub>3</sub> or pdmH<sub>2</sub> were employed, the reaction instead comprising the methanolysis of a Mn<sup>III</sup> species in the presence of a Yb<sup>3+</sup> or Y<sup>3+</sup> source. The chosen Mn starting material was the readily prepared, tetranuclear (NBu<sub>4</sub>)<sub>4</sub>[Mn<sub>4</sub>O<sub>2</sub>(O<sub>2</sub>CPh)<sub>9</sub>(H<sub>2</sub>O)] (4Mn<sup>III</sup>) complex [25], and treatment of this with Yb(NO<sub>3</sub>)<sub>3</sub> · 5H<sub>2</sub>O in a 1:2 molar ratio in MeCN/MeOH led to brown crystals of  $[Mn_2Y_2O_2(O_2CPh)_6(OMe)_4(MeOH)_4]$  (**6**) or  $[Mn_2Yb_2O_2(O_2CPh)_6(OMe)_4(MeOH)_4]$  (**7**) in 10–25% yields. Note that in both these Mn-containing complexes that there are also MeO<sup>-</sup> groups from the MeOH solvent, whereas none of the

Fe-containing complexes **1–5** contain MeO<sup>-</sup> groups. Again, there are likely other products from these complicated reactions in the colored filtrates, but we have not pursued any further separations.

#### 3.2. Structural description of

##### $[Fe_2Ho_2(OH)_2(teaH)_2(O_2CPh)_4(NO_3)_2]$ (**1**)

A labeled ORTEP plot and stereoview of the  $[Fe_2Ho_2(OH)_2(teaH)_2(O_2CPh)_4(NO_3)_2]$  (**1**) are provided in Fig. 1. Selected bond distances and angles are listed in Table 2. Complex **1** · 6MeCN crystallizes in triclinic space group  $P\bar{1}$ , the cluster lying on an inversion center and consisting of a planar Fe<sub>2</sub>Ho<sub>2</sub> rhombus. Each Fe<sub>2</sub>Ho trinuclear sub-unit is bridged by a μ<sub>3</sub>-OH<sup>-</sup> ion (oxygen atoms O1 and O1a). Each of the two teaH<sup>2-</sup> ligands binds in a tetradentate chelate fashion to Ho1 or Ho1a, with their protonated alcohol arms (O8 and O8a) binding terminally to the Ho, and their two deprotonated alkoxide arms each bridging to an adjacent Fe atom (O3 bridging Fe1/Ho1, and O5 bridging Fe1a/Ho1). There is also a chelating NO<sub>3</sub><sup>-</sup> group on each Ho atom, and ligation is completed by a *syn, syn*, bridging benzoate group across each of the four HoFe edges of the rhombus. The Fe and Ho atoms are six- and nine-coordinate, respectively.

The overall structure of the core of complex **1** can be described as two face-sharing  $[M_4O_4]$  cubanes with a metal atom missing from one vertex in each cubane. Such a ‘defect double-cubane’ unit with a resulting planar M<sub>4</sub> rhombus is relatively common in both homo- and heterometallic cluster chemistry, and is often on a crystallographic center of symmetry. Such examples are known

Table 2  
Selected bond distances (Å) and angles (°) for complex **1**

Fe1...Fe1a	3.243(6)
Fe1...Ho1	3.3935(6)
Fe1...Ho1a	3.4027(6)
Fe1–O1	2.067(3)
Fe1–O2	2.031(3)
Fe1–O3	1.943(3)
Fe1–O4a	2.002(3)
Fe1–O5a	1.972(3)
Fe1–O1a	2.044(3)
Ho1–O1a	2.356(3)
Ho1–O3	2.293(3)
Ho1–O5	2.313(3)
Ho1–O6	2.329(3)
Ho1–O7	2.408(3)
Ho1–O8	2.414(3)
Ho1–O9	2.494(3)
Ho1–O10	2.514(3)
Ho1–N1	2.572(3)
Ho1–N2	2.911(4)
Fe1a–O1–Fe1	104.13(12)
Fe1a–O1–Ho1a	100.68(12)
Fe1–O1–Ho1a	100.35(12)
Fe1–O3–Ho1	106.18(12)
Fe1a–O5–Ho1	104.87(12)

with different transition metals [28,33], and there are also a very few examples of mixed 3d/4f examples [14b,34], but no mixed iron–lanthanide complexes have previously been obtained. We also carried out preliminary X-ray crystallographic studies on complexes **2** and **3** and found that they are isostructural with **1** except that the two chelating  $\text{NO}_3^-$  groups have been replaced by two chelating  $\text{PhCO}_2^-$  groups, as we had suspected from the similar formulas and IR spectra of **1**–**3**. For this reason, the structures of **2** and **3** will not be discussed further here.

### 3.3. Structural descriptions of $[\text{Fe}_2\text{Y}_2(\text{pdmH})_6\text{Cl}_4]\text{Cl}_2$ (**4**) and $[\text{Fe}_2\text{Ho}_2(\text{pdmH})_6\text{Cl}_4]\text{Cl}_2$ (**5**)

Labeled ORTEP plots and stereoviews of the cations of complexes **4** · 2MeOH and **5** · 2MeOH are shown in Figs. 2 and 3, respectively. Selected bond lengths and angles are listed in Tables 3 and 4, respectively. The complexes both crystallize in monoclinic space group  $I2/a$ , with the cations on a crystallographic  $C_2$  rotation axis; the two complexes are isostructural. The cores of the cations (Fig. 4) can best

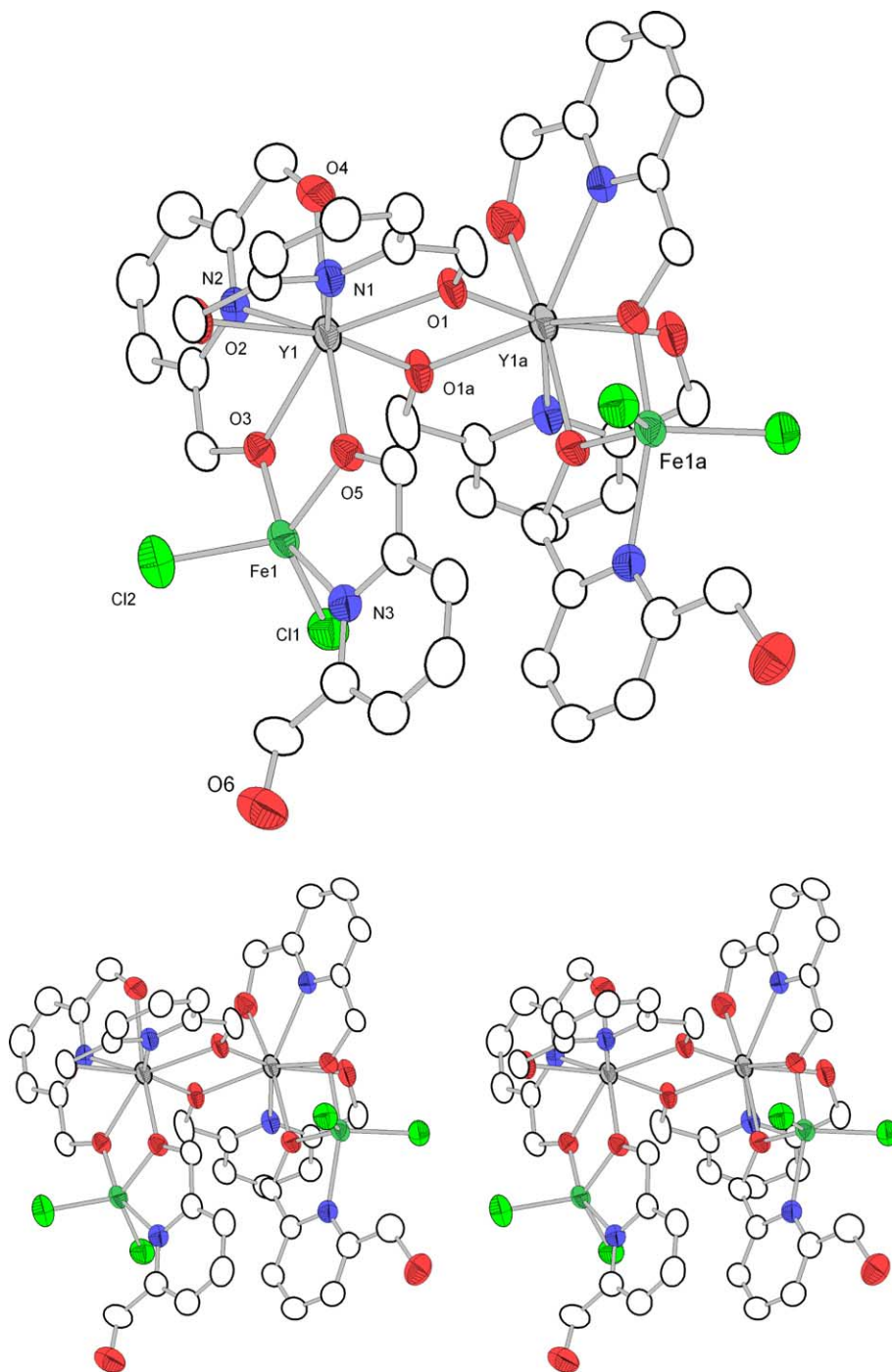


Fig. 2. ORTEP representation and stereopair of the cation of complex **4** at the 50% probability level. All H atoms have been removed for clarity.

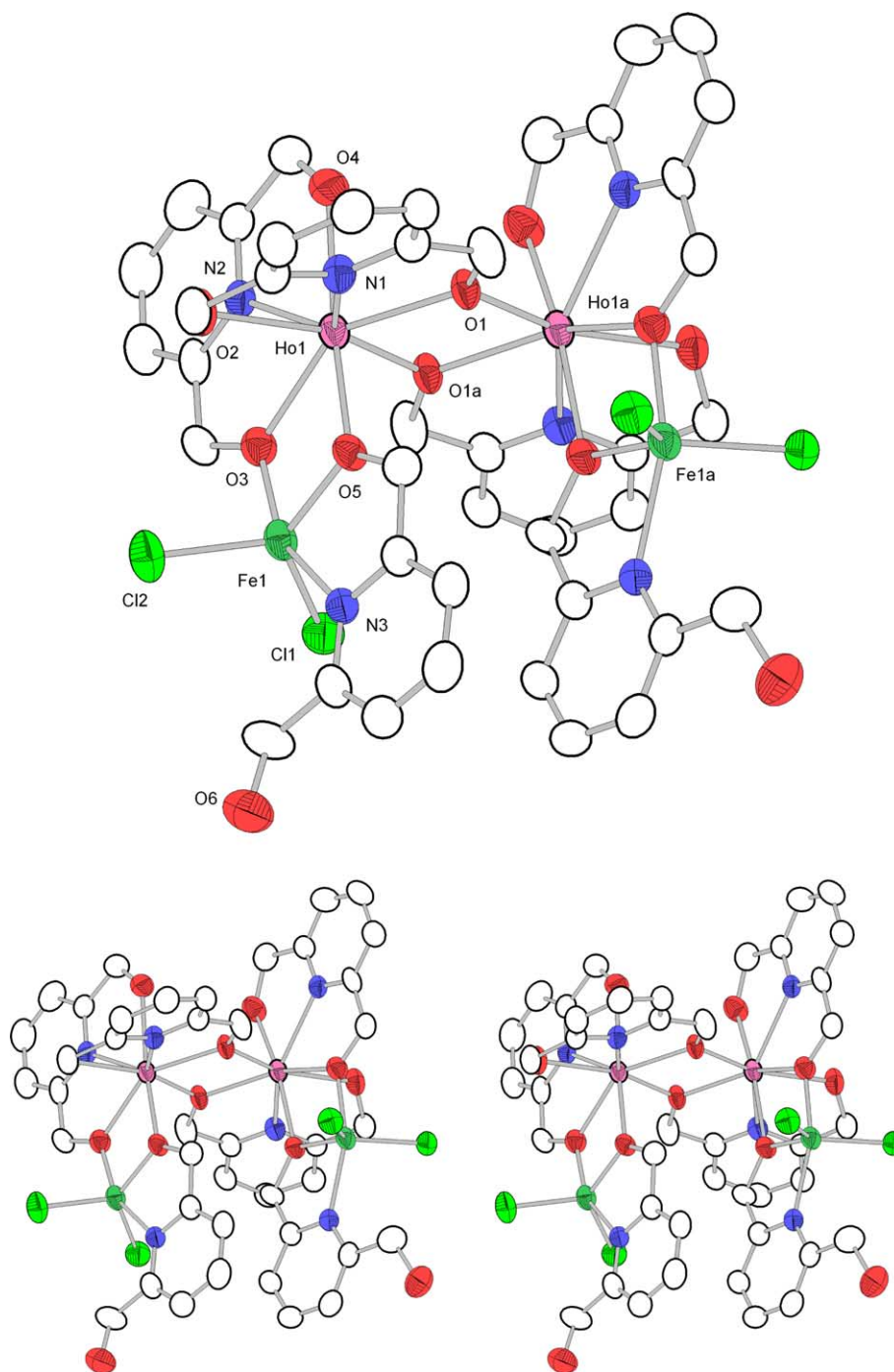


Fig. 3. ORTEP representation and stereopair of the cation of complex **5** at the 50% probability level. All H atoms have been removed for clarity.

be described as twisted U-shaped, with the  $\text{Fe}^{\text{III}}$  atoms at the two ends, and either two  $\text{Y}^{\text{III}}$  (complex **4**) or two  $\text{Ho}^{\text{III}}$  (complex **5**) atoms on the inside. Each pair of adjacent metal atoms is bridged by two alkoxide O atoms from mono-deprotonated pdmH<sup>-</sup> groups. There are two of the latter as tridentate chelates on each of the inner  $\text{Y}^{\text{III}}$  (**4**) or  $\text{Ho}^{\text{III}}$  (**5**) atoms, with their alkoxide arm bridging to an adjacent atom (O1, O3), as mentioned, and their protonated (alcohol) arm (O2, O4) and N atom binding terminally. There are two additional pdmH<sup>-</sup> groups, attached in a bidentate chelate fashion to the  $\text{Fe}^{\text{III}}$  atoms, their alkoxide arm (O5)

bridging to an inner metal and their protonated arm unligated (O6). Ligation is completed by two terminal  $\text{Cl}^-$  ions on each of the  $\text{Fe}^{\text{III}}$  atoms. The two Fe atoms are five-coordinate and the two inner  $\text{Y}^{\text{III}}$  or  $\text{Ho}^{\text{III}}$  atoms are eight-coordinate. There are intramolecular  $\pi$ - $\pi$  stacking interactions, and many intermolecular hydrogen-bonds involving the pdmH<sup>-</sup>, MeOH and  $\text{Cl}^-$  groups, the latter serving to bridge separate  $\text{Fe}_2\text{Y}_2(\text{Ho})_2$  clusters. For example for **4**, the unbound pdmH<sup>-</sup> alcohol group (O6) hydrogen-bonds to interstitial MeOH atom O7 (O6...O7 = 2.695 Å), with the latter also hydrogen-bonding to free

Table 3  
Selected bond distances (Å) and angles (°) for complex 4

Y1...Fe1	3.4487(6)
Y1...Y1a	3.7121(7)
Y1–O1	2.283(2)
Y1–O1a	2.252(2)
Y1–O2	2.416(3)
Y1–O3	2.316(2)
Y1–O4	2.374(3)
Y1–O5	2.329(2)
Y1–N1	2.466(3)
Y1–N2	2.480(3)
Fe1–O3	1.943(2)
Fe1–O5	1.926(2)
Fe1–N3	2.218(3)
Fe1–Cl1	2.2541(10)
Fe1–Cl2	2.2209(11)
Y1–O1–Y1a	109.87(9)
Fe1–O3–Y1	107.80(9)
Fe1–O5–Y1	107.94(10)

Table 4  
Selected bond distances (Å) and angles (°) for complex 5

Ho1...Ho1a	3.7153(5)
Ho1...Fe1	3.4702(9)
Ho1–O1	2.286(3)
Ho1–O1a	2.248(3)
Ho1–O2	2.419(4)
Ho1–O3	2.325(3)
Ho1–O4	2.375(4)
Ho1–O5	2.316(4)
Ho1–N1	2.462(4)
Ho1–N2	2.482(4)
Fe1–O3	1.983(4)
Fe1–O5	1.928(3)
Fe1–N3	2.211(4)
Fe1–Cl1	2.2532(15)
Fe1–Cl2	2.2331(16)
Ho1–O1–Ho1a	110.04(13)
Fe1–O3–Ho1	107.04(14)
Fe1–O5–Ho1	109.35(15)

Cl<sup>−</sup> ion Cl3 (O7...Cl3 = 3.072 Å). In addition, this Cl<sup>−</sup> ion hydrogen-bonds to bound pdm<sup>2−</sup> O atom O2 (Cl3...O2 = 2.976 Å) of a neighboring cluster.

The U-shaped core seen in these complexes is not common, although it is with precedent, for example in the complex [Mn<sub>4</sub>(6Me-hmp)Cl<sub>4</sub>]·4H<sub>2</sub>O (6Me-hmp = 6-methyl-2-(hydroxymethyl)pyridine) [35].

### 3.4. Structural descriptions of

[Mn<sub>2</sub>Y<sub>2</sub>O<sub>2</sub>(O<sub>2</sub>CPh)<sub>6</sub>(OMe)<sub>4</sub>(MeOH)<sub>4</sub>] (6) and  
[Mn<sub>2</sub>Yb<sub>2</sub>O<sub>2</sub>(O<sub>2</sub>CPh)<sub>6</sub>(OMe)<sub>4</sub>(MeOH)<sub>4</sub>] (7)

Labeled ORTEP representations of the centrosymmetric structures of 6·2MeOH and 7·2MeOH are presented in Fig. 5, and selected bond distances and angles are listed in Table 5. The two complexes both crystallize in the monoclinic space group *P*<sub>2</sub><sub>1</sub>/*c* with the molecules lying on an inversion center; the two complexes are isostructural. The cores of the complexes possess the defect-dicubane

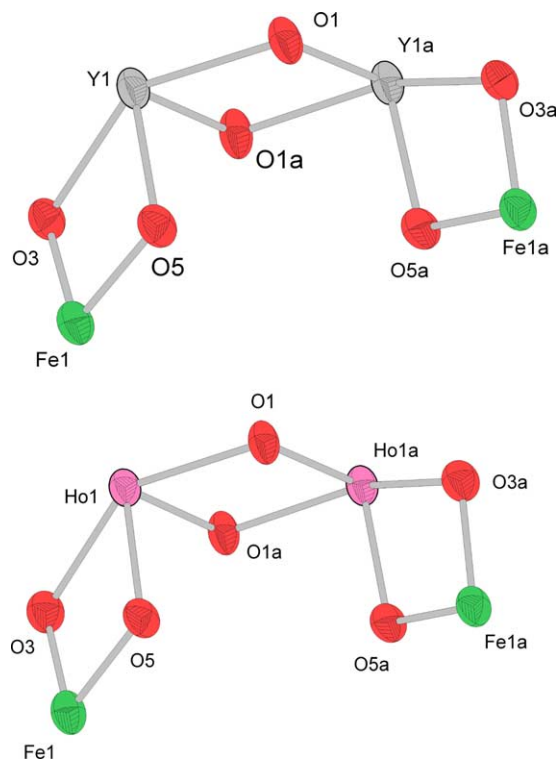


Fig. 4. Comparison of the cores of the cations of complexes 4 (top) and 5 (bottom).

structure of complex 1, with two Mn<sup>IV</sup> atoms at the central positions and either two 2Y<sup>III</sup> (complex 6) or two Yb<sup>III</sup> (complex 7) atoms at the end positions. However, there are two major differences between the cores of 6/7 and that of 1: First, the two μ<sub>3</sub>-O atoms (O8, O8a) capping each triangular sub-unit are O<sup>2−</sup> ions rather than OH<sup>−</sup> ones; and secondly, each of the four edges of the M<sub>4</sub> rhombus in 6/7 is bridged by a MeO<sup>−</sup> ion (O7, O7a, O11, O11a) rather than an alkoxide arm of a chelate. The fully labeled cores of 6 and 7 are provided in Fig. 6, which emphasize the near superimposability of the mixed 3d/4d complex 6 with the mixed 3d/4f complex 7. Peripheral ligation about the cores is provided by four *syn*, *syn* bridging benzoate groups bridging each Y/Mn or Yb/Mn edge of the rhombus, two monodentate benzoate groups, one on each of the Y/Yb atoms, and four terminal MeOH molecules, two on each of the Y/Yb ions. As a result, the Y<sup>III</sup> and Yb<sup>III</sup> atoms of 6 and 7, respectively, are eight-coordinate, and the Mn<sup>IV</sup> atoms are six-coordinate. There are intramolecular OH...H hydrogen bonds between the unbound O atom (O1) and the terminal MeOH ligand (O1...O10 = 2.577 Å). In addition, there are intermolecular OH...H hydrogen bonds between the bound MeOH (O9) and interstitial MeOH (O12) molecules (O9...O12 = 2.656 Å), and between this interstitial MeOH and the unbound O atom (O1) of a neighboring cluster (O12...O1 = 2.687 Å). Thus, the hydrogen-bonding through the interstitial MeOH molecules links adjacent metal clusters in the crystal, which also likely provides a pathway for superexchange interactions between molecules (*vide infra*).

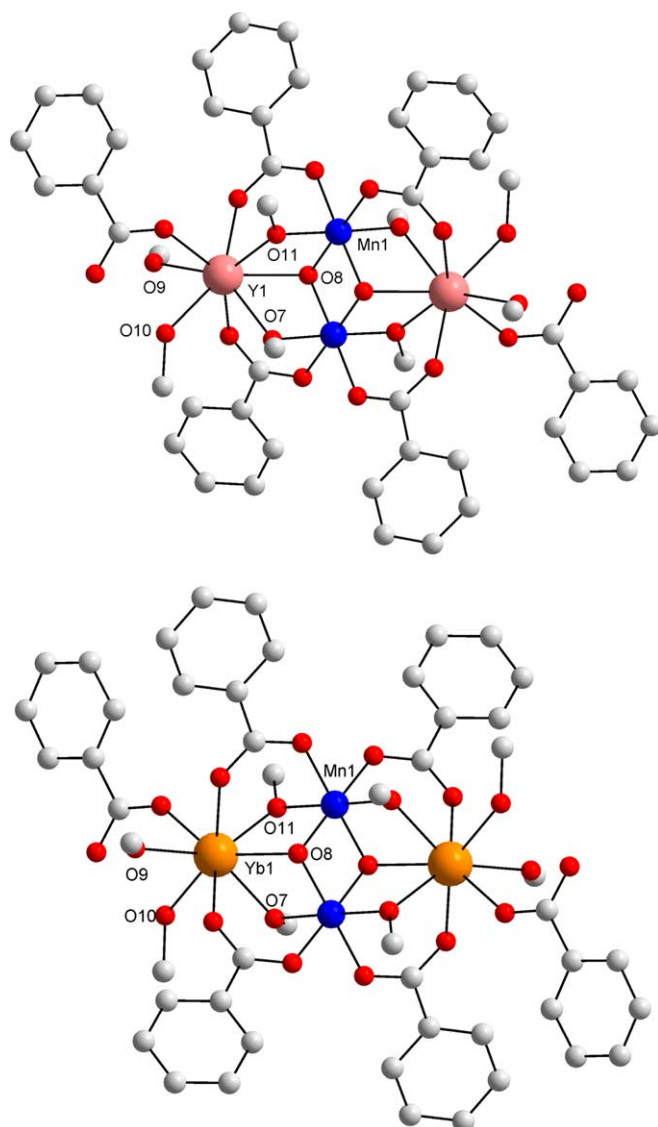


Fig. 5. PovRay representations of complexes **6** (top) and **7** (bottom).

It should be noted that mixed  $Mn_2Ln_2$  complexes with the same kind of defect-dicubane core have previously been reported for  $Ln = Dy, Gd$  and  $Tb$  [14b,34]. However, in all of these previous cases, the Mn atoms were in the  $Mn^{III}$  oxidation state, so **6** and **7** are the first to instead contain  $Mn^{IV}$ . The  $Mn^{IV}$  oxidation level is suggested by overall charge considerations and inspection of metric parameters; in particular, Mn–O bond distances all lie in the range 1.84–1.97 Å, as expected for  $Mn^{IV}$ , and thus do not show the Jahn-Teller axial distortion expected for  $Mn^{III}$  in near octahedral geometry. The Y–O and Yb–O bond distances are very similar, lying in the 2.30–2.42 and 2.27–2.38 Å ranges, respectively, consistent with eight-coordinate  $Y^{III}/Yb^{III}$  centers. The  $Mn^{IV}$  oxidation states and the protonation levels of the  $O^{2-}$ ,  $MeO^-$  and  $MeOH$  were confirmed by bond valence sum (BVS) calculations, shown in Tables 6 and 7. The BVS values for the Mn atoms are clearly  $\sim 4$ , confirming the  $Mn^{IV}$  oxidation level. Values of  $\sim 2$  are expected for O atoms in the  $O^{II-}$  oxidation level and that

Table 5  
Selected bond distances (Å) and angles ( $^\circ$ ) for complexes **6** and **7**

Complex 6	
Y1···Mn1	3.3168(7)
Mn1···Mn1a	2.7819(9)
Y1–O7	2.365(2)
Y1–O8	2.356(2)
Y1–O9	2.416(2)
Y1–O10	2.351(2)
Y1–O11	2.299(2)
Mn1–O8	1.859(2)
Mn1–O11	1.913(2)
Y1–O11–Mn1	102.08(9)
Mn1–O8–Mn1a	97.52(9)
Y1–O8–Mn1	103.18(9)
Complex 7	
Yb1···Mn1	3.2886(6)
Mn1···Mn1a	2.7769(11)
Yb1–O7	2.336(2)
Yb1–O8	2.331(2)
Yb1–O9	2.383(3)
Yb1–O10	2.323(3)
Yb1–O11	2.269(2)
Mn1–O8	1.866(2)
Mn1–O11	1.912(3)
Yb1–O11–Mn1	101.79(11)
Mn1–O8–Mn1a	97.05(11)
Yb1–O8–Mn1	102.61(10)

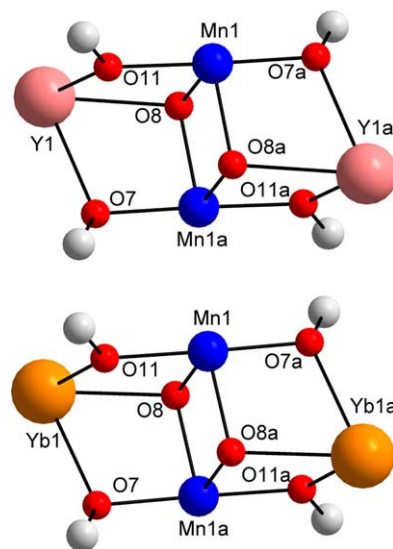


Fig. 6. Comparison of the cores of complexes **6** (top) and **7** (bottom), emphasizing their near superimposability.

have no attached atoms that cannot be seen in X-ray crystallography (i.e., H atoms). This confirms that O7, O8 and O11 are  $MeO^-$ ,  $O^{2-}$ , and  $MeO^-$ , respectively. In contrast, if there is a H atom which is not visible and its contribution to the BVS of that O atom is therefore not included, a lower BVS value is expected, typically 1–1.5 (depending on the degree of its participation in hydrogen-bonding); this is clearly the case for O9 and O10, which are therefore confirmed as  $MeOH$  groups.

Table 6  
Bond valence sums (BVS)<sup>a</sup> for the Mn atoms of complexes **6** (Y) and **7** (Yb)

Atom	Mn <sup>II</sup>	Mn <sup>III</sup>	Mn <sup>IV</sup>	Assignment
Mn1 ( <b>6</b> )	4.132	3.779	<u>3.967</u>	Mn <sup>IV</sup>
Mn1 ( <b>7</b> )	4.124	3.772	<u>3.959</u>	Mn <sup>IV</sup>

<sup>a</sup> The underlined value is the one closest to the charge for which it was calculated. The oxidation state of a particular metal is the nearest whole number to that value.

Table 7  
Bond valence sums (BVS) for the O atoms of complexes **6** (Y) and **7** (Yb)

Atom	BVS ( <b>6</b> )	BVS ( <b>7</b> )	Assignment
O7	1.972	1.972	MeO <sup>-</sup>
O8	1.898	1.859	O <sup>2-</sup>
O9	1.210	1.198	MeOH
O10	1.339	1.342	MeOH
O11	2.038	2.016	MeO <sup>-</sup>

The occurrence of Mn<sup>IV</sup> in **6** and **7** is noteworthy given that the reaction employed a Mn<sub>4</sub><sup>III</sup> starting material and either Y<sup>III</sup> or Yb<sup>III</sup>, neither of which are good oxidizing agents. This points to either the participation of atmospheric O<sub>2</sub> gas as the oxidizing agent or the disproportionation of Mn<sup>III</sup> to Mn<sup>IV</sup> and Mn<sup>II</sup>. We favor the latter possibility given the low yields of these complexes, but we have not sought Mn<sup>II</sup> species in the filtrates to confirm this.

## 4. Magnetochemistry

### 4.1. DC magnetic susceptibility

The magnetic properties of **1–6** were investigated by solid state magnetic susceptibility ( $\chi_M$ ) measurements in the 5.0–300 K range in a 0.1 tesla (T) DC field. The resulting data for complexes **1–3**, **4–5** and **6** are shown as  $\chi_M T$  versus  $T$  plot in Figs. 7–9, respectively. For complex **1**, the  $\chi_M T$  value of 33.1 cm<sup>3</sup> K mol<sup>-1</sup> at 300 K is slightly less than the value expected for 2Fe<sup>III</sup> ( $S = 5/2$ ,  $g = 2$ ) and 2Ho<sup>III</sup> ( $S = 2$ ,  $L = 6$ , <sup>5</sup>I<sub>8</sub>) non-interacting ions of 36.9 cm<sup>3</sup> K mol<sup>-1</sup>, consistent with antiferromagnetic exchange interactions, and decreases steadily to 24.2 cm<sup>3</sup> kmol<sup>-1</sup> at 50 K and then 13.7 cm<sup>3</sup> kmol<sup>-1</sup> at 5.0 K. Complexes **2** and **3** behave in a similar fashion to complex **1**. For complex **2**, the  $\chi_M T$  value of 37.1 cm<sup>3</sup> kmol<sup>-1</sup> at 300 K is essentially that expected for 2Fe<sup>III</sup> ( $S = 5/2$ ,  $g = 2$ ) and 2Dy<sup>III</sup> ( $S = 5/2$ ,  $L = 5$ , <sup>6</sup>H<sub>15/2</sub>) non-interacting ions of 36.94 cm<sup>3</sup> kmol<sup>-1</sup>, and it decreases with decreasing temperature to 30.3 cm<sup>3</sup> kmol<sup>-1</sup> at 50 K, and then to 23.8 cm<sup>3</sup> kmol<sup>-1</sup> at 5.0 K. For complex **3**, the  $\chi_M T$  value of 35.5 cm<sup>3</sup> kmol<sup>-1</sup> at 300 K is slightly greater than that expected for 2Fe<sup>III</sup> ( $S = 5/2$ ,  $g = 2$ ) and 2Tb<sup>III</sup> ( $S = 3$ ,  $L = 3$ , <sup>7</sup>F<sub>6</sub>) non-interacting ions of 32.4 cm<sup>3</sup> kmol<sup>-1</sup>, and it decreases with decreasing temperature to 29.1 cm<sup>3</sup> kmol<sup>-1</sup> at 50 K, and then to 22.4 cm<sup>3</sup> kmol<sup>-1</sup> at 5.0 K. The data suggest predominantly antiferromagnetic exchange interactions within all three

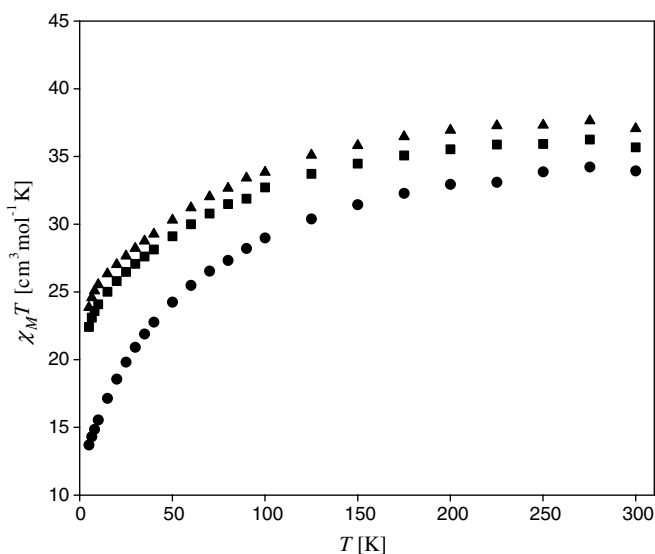


Fig. 7. Plot of  $\chi_M T$  vs.  $T$  for complexes **1** (●), **2** (▲) and **3** (■).

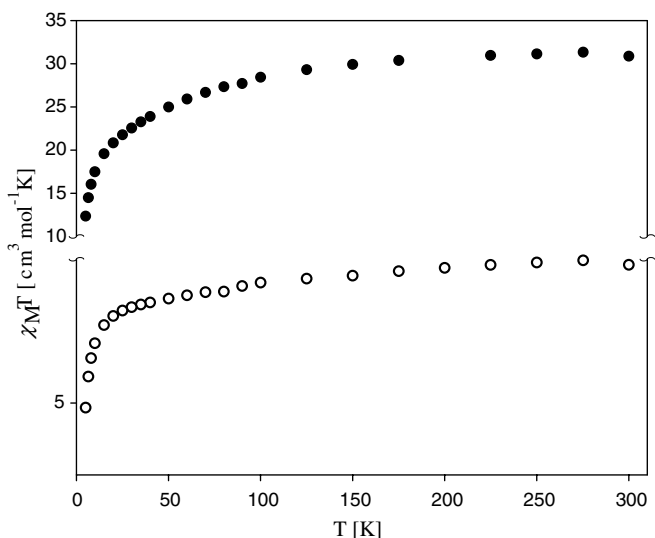


Fig. 8. Plot of  $\chi_M T$  vs.  $T$  for complexes **4** (○) and **5** (●).

complexes, but with perhaps some ferromagnetic contributions. The presence of strong spin–orbit coupling effects in these three lanthanide derivatives makes the fitting of the data to obtain Fe<sup>III</sup>Fe<sup>III</sup> and Fe<sup>III</sup>Ln<sup>III</sup> exchange parameters far from straightforward. Such an analysis would in fact greatly benefit from the availability and parallel study of the corresponding Gd<sup>3+</sup> ( $S = 7/2$ ,  $L = 0$ ) and Y<sup>3+</sup> ( $S = 0$ ) derivatives, but unfortunately neither of these are available at the present time. A more complete magnetic analysis of complexes **1–3** and other derivatives is thus the objective of future work.

Complex **4** has a  $\chi_M T$  value at 300 K of 6.9 cm<sup>3</sup> kmol<sup>-1</sup> which is less than that expected for two non-interacting Fe<sup>III</sup> centers of 8.8 cm<sup>3</sup> kmol<sup>-1</sup> with  $g = 2$ , and it decreases only slightly with decreasing temperature to 6.3 cm<sup>3</sup> kmol<sup>-1</sup> at 35 K, but then much more rapidly to 4.9 cm<sup>3</sup> kmol<sup>-1</sup> at 5.0 K (Fig. 8). This behavior is probably due to a very weak

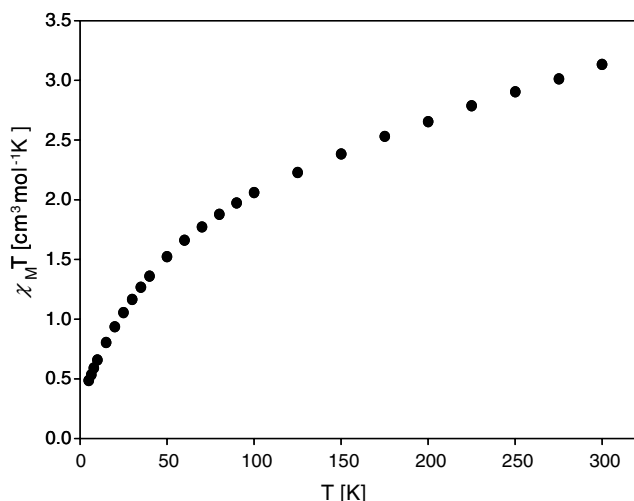


Fig. 9. Plot of  $\chi_M T$  vs.  $T$  for complex **6**.

antiferromagnetic exchange interaction between the  $\text{Fe}^{\text{III}}$  ions via the intervening, diamagnetic  $\text{Y}^{\text{III}}$  ions, but we cannot get a good fit of the data over the entire temperature range to the Van Vleck equation for a  $S_1 = S_2 = 5/2$  dimer. We suspect this is due to the exchange interaction being so weak as a result of the large separation between  $\text{Fe}^{\text{III}}$  atoms that it is thus comparable in magnitude to intermolecular interactions mediated by the multiple intermolecular hydrogen-bonds between adjacent clusters, as described above. Complex **5** has a  $\chi_M T$  value of  $30.8 \text{ cm}^3 \text{ kmol}^{-1}$  at 300 K, which, as for **1**, is again less than the  $36.9 \text{ cm}^3 \text{ kmol}^{-1}$  expected for two  $\text{Fe}^{\text{III}}$  ( $S = 5/2$ ) and two  $\text{Ho}^{\text{III}}$  ( $S = 2$ ,  $L = 6$ ,  $^5\text{I}_8$ ) non-interacting ions; it then decreases to  $28.4 \text{ cm}^3 \text{ kmol}^{-1}$  at 100 K, and then more rapidly to  $20.8 \text{ cm}^3 \text{ kmol}^{-1}$  at 20 K then finally to  $12.3 \text{ cm}^3 \text{ kmol}^{-1}$  at 5.0 K (Fig. 8). The overall behavior is consistent with antiferromagnetic exchange interactions between the constituent metal atoms.

Complex **6** has a  $\chi_M T$  value that steadily decreases almost linearly from  $3.13 \text{ cm}^3 \text{ kmol}^{-1}$  at 300 K to  $1.52 \text{ cm}^3 \text{ kmol}^{-1}$  at 50 K, and then more rapidly decreases to  $0.49 \text{ cm}^3 \text{ kmol}^{-1}$  at 5.0 K (Fig. 9). The value at 300 K is less than the expected spin-only ( $g = 2$ ) value for a complex consisting of two non-interacting  $\text{Mn}^{\text{IV}}$  ions ( $S = 3/2$ ; the  $2\text{Y}^{\text{III}}$  ions are diamagnetic) of  $3.75 \text{ cm}^3 \text{ kmol}^{-1}$ , indicating an antiferromagnetic exchange interaction between the  $\text{Mn}^{\text{IV}}$  ions and a resultant  $S = 0$  spin ground state. Attempts to fit the  $\chi_M T$  versus  $T$  data using the isotropic Heisenberg–Dirac–van Vleck Hamiltonian described by  $\mathcal{H} = -2J\hat{S}_1\hat{S}_2$ , where  $S_1 = S_2 = 3/2$  and  $J$  is the magnetic exchange interaction gave poor fits that did not reproduce the data over the whole temperature range, particularly the higher  $T$  data. However, it did suggest the  $J$  value is relatively weak, in the  $J = -10$  to  $-15 \text{ cm}^{-1}$  range, which in fact is consistent with the relatively acute  $\text{Mn}^{4+}\text{–O}^{2-}\text{–Mn}^{4+}$  ( $\text{Mn1–O8–Mn1a}$ ) angles of  $97.52^\circ$ . As for **4**, we believe the problem is intermolecular exchange interactions, via the hydrogen-bonding network described above,

which are not incorporated in the model. These points are being considered further as we seek to reach a more detailed magnetic understanding of this whole family of mixed-metal species, as well as others being prepared.

#### 4.2. AC magnetic susceptibility

AC magnetic susceptibility measurements are a very convenient method to assess whether a molecule exhibits a slow magnetization relaxation rate, which is a necessary (but not sufficient) property of a species that might be a single-molecule magnet (SMM). Thus, such measurements were carried out in the 1.8–10 K range using a 3.5 G AC field oscillating at 50–1000 Hz, seeking the detection of a non-zero out-of-phase AC susceptibility signal ( $\chi_M''$ ). The latter indicates that the sample's magnetization vector cannot relax (reorient) fast enough to keep up with the oscillating field. None of the complexes in this work gave a clear  $\chi_M''$  signal above 1.8 K, the operating minimum of our SQUID magnetometer, but complex **2** showed a weak, frequency-dependent tail of what might be a peak lying at  $<1.8$  K. We thus chose **1** and **2** for more detailed studies involving single-crystal magnetization versus applied DC field sweeps on a micro-SQUID apparatus down to millikelvin temperatures [26]. The observation of hysteresis loops in such studies is the classical diagnostic property of a magnet.

The magnetization versus applied DC field sweeps for a single crystal of complex **1** · 6MeCN are shown in Fig. 10. At very low temperatures (0.3 K and below) and at a 0.14 T/s applied field sweep rate, hysteresis loops are observed with a very small coercivity and only a slight temperature dependence. The small coercive field and the overall shape of the loops suggest the presence of intermolecular interactions and some degree of ordering as the main source of the hysteresis. Indeed, a closer examination

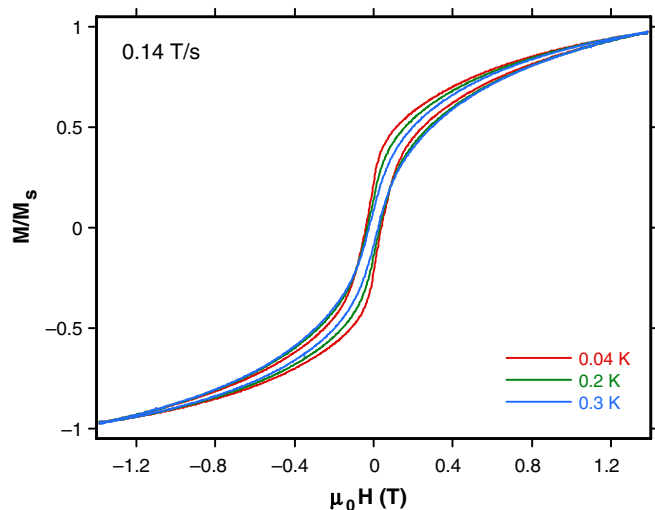


Fig. 10. Magnetization ( $M$ ) vs. applied DC field hysteresis loops for a single crystal of **1** · 6MeCN at the indicated temperatures and a 0.14 T/s sweep rate. The magnetization is normalized to its saturation value,  $M_S$ .

of the crystal structure of  $\mathbf{1} \cdot 6\text{MeCN}$  reveals intermolecular  $\pi$ – $\pi$  stacking overlaps ( $\sim 3.7$  Å) between the aromatic rings of benzoate groups, and this is likely the pathway for intermolecular exchange interactions. At best, therefore, complex  $\mathbf{1}$  could be regarded as an exchange-biased SMM [36], although it is clearly difficult to separate the intermolecular interactions and the SMM behavior.

Clearer evidence for a SMM was observed when the same studies were performed on  $\mathbf{2} \cdot 4\text{MeCN} \cdot 3\text{H}_2\text{O}$ . Hysteresis loops were again obtained, and now they were much more characteristic of a SMM. The hysteresis loops obtained with a field sweep rate of 0.14 T/s and at various temperatures below 1.1 K are shown in Fig. 11 (top), and those obtained from a sweep rate dependence at a constant temperature of 0.04 K are shown in Fig. 11 (bottom). The coercivities increase with decreasing temperature and with increasing sweep rate, as expected for the superparamag-

net-like behavior of a SMM. The dominating feature in these loops is the large relaxation step at zero-field, which can be assigned to fast quantum tunneling of the magnetization (QTM) through the barrier to relaxation. This is commonly seen in previous SMMs containing lanthanide ions [14b]. In fact, this very fast QTM step at zero field makes the magnetization decay very rapidly in zero field and prevents magnetization versus time decay data being collected and used to construct an Arrhenius plot; the latter kinetic analysis is commonly used to determine the effective barrier to relaxation. Again, this is as found for previous mixed 3d/4f SMMs, which show fast QTM at zero field. Steps at other field positions are also expected, but they are poorly resolved, almost unobservable, and this is assigned to broadening effects from a distribution of molecular environments, which would give a distribution of relaxation barriers and thus a distribution in step positions. Additional broadening is also expected from intermolecular interactions from both dipolar and superexchange pathways.

## 5. Conclusions

A new group of mixed 3d/4f and 3d/4d tetranuclear clusters have been synthesized from the reactions of  $\text{Fe}^{\text{III}}$  or  $\text{Mn}^{\text{III}}$  sources with  $\text{teaH}_3$  or  $\text{pdmH}_2$ , or simply by methanolysis. These products represent new additions to what is still a very small family of such mixed-metal species. While the magnetic properties are complicated by the large spin–orbit coupling effects of most  $\text{Ln}^{\text{III}}$  ions, making difficult the quantitative elucidation of the magnitude of the exchange parameters within these molecules and their resulting ground state description, hysteresis loop determinations have established that additional examples of SMMs have been provided from this area. However, lanthanide-containing SMMs still suffer from the disadvantage of fast QTM rates. This represents a diminution of the effective barrier for magnetization relaxation, and thus the temperature below which the relaxation is blocked and the complex will function as a SMM. Nevertheless, the use of lanthanides to modulate the magnetic properties of transition metal SMMs is still an interesting area that promises much new science as it matures.

## 6. Supplementary material

Crystallographic data have been deposited with Cambridge Crystallographic Data centre, CCDC Nos. 276642–276646. Copies of this information may be obtained from The Director, CCDC, 12 Union Road, Cambridge, CB2 1EZ, UK (fax: +44 1233 336033; email: deposit@ccdc.cam.ac.uk or [www.ccdc.cam.ac.uk](http://www.ccdc.cam.ac.uk)).

## Acknowledgment

This work was supported by the National Science Foundation.

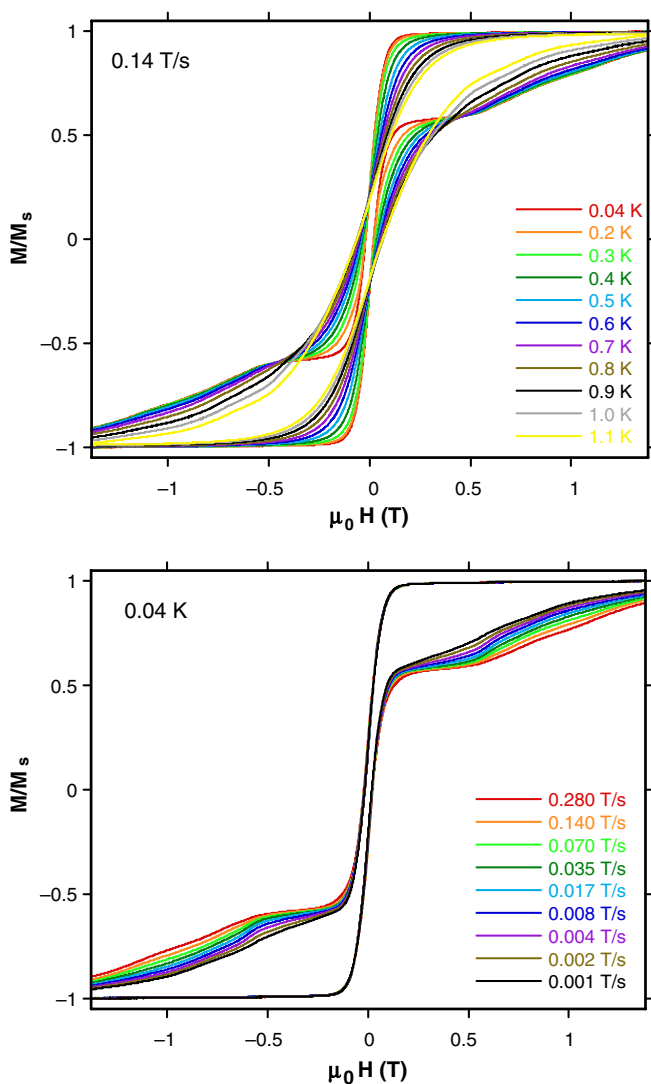


Fig. 11. Magnetization ( $M$ ) vs. applied DC field hysteresis loops for a single crystal of  $\mathbf{2} \cdot 4\text{MeCN} \cdot 3\text{H}_2\text{O}$  at (top) the indicated temperatures and a 0.14 T/s sweep rate, and (bottom) at the indicated field sweep rates and a temperature of 0.04 K. The magnetization is normalized to its saturation value,  $M_S$ .

## References

- [1] G. Christou, D. Gatteschi, D.N. Hendrickson, R. Sessoli, *MRS Bull.* 25 (2000) 66.
- [2] R. Sessoli, H. Tsai, A.R. Schake, S. Wang, J.B. Vincent, K. Folting, D. Gatteschi, G. Christou, D.N. Hendrickson, *J. Am. Chem. Soc.* 115 (1993) 1804.
- [3] M. Soler, W. Wernsdorfer, K.A. Abboud, D.N. Hendrickson, G. Christou, *Polyhedron* 22 (2003) 1777.
- [4] E.C. Theil, *Annu. Rev. Biochem.* 57 (1987) 289, and references therein.
- [5] B. Xu, N.D. Chasteen, *J. Biol. Chem.* 266 (1991) 19965.
- [6] R.A. Grant, D.J. Filman, S.E. Finkel, R. Kolter, J. Hogle, *Nat. Struct. Biol.* 5 (1998) 294.
- [7] (a) V.K. Yachandra, K. Sauer, *Biochim. Biophys. Acta* 1655 (2004) 140;  
(b) K.N. Ferreira, T.M. Iverson, K. Maghlaoui, J. Barber, S. Iwata, *Science* 303 (2004) 1831.
- [8] A. Mishra, W. Wernsdorfer, K.A. Abboud, G. Christou, *Chem. Commun.* (2005) 54.
- [9] R. Sessoli, D. Gatteschi, A. Caneschi, M.A. Novak, *Nature* 365 (1993) 141.
- [10] S.M. Aubin, N.R. Gilley, L. Pardi, J. Krzystek, M.W. Wemple, L.C. Brunel, M.B. Marple, G. Christou, D.N. Hendrickson, *J. Am. Chem. Soc.* 120 (1998) 4991.
- [11] S.M. Aubin, M.W. Wemple, D.M. Adams, H.-L. Tsai, G. Christou, D.N. Hendrickson, *J. Am. Chem. Soc.* 118 (1996) 7746.
- [12] E.K. Brechin, J. Yoo, J.C. Huffman, D.N. Hendrickson, G. Christou, *Chem. Commun.* (1999) 783.
- [13] (a) G. Aromi, S.M.J. Aubin, M.A. Bolcar, G. Christou, H.J. Eppley, K. Folting, D.N. Hendrickson, J.C. Huffman, R.C. Squire, H.-L. Tsai, S. Wang, M.W. Wemple, *Polyhedron* 17 (1998) 3005;  
(b) G. Christou, *Polyhedron* (in press), and references therein.
- [14] (a) A. Mishra, W. Wernsdorfer, K.A. Abboud, G. Christou, *J. Am. Chem. Soc.* 126 (2004) 15648;  
(b) A. Mishra, W. Wernsdorfer, S. Parsons, G. Christou, E.K. Brechin, *Chem. Commun.* (2005) 2086;  
(c) A.J. Tasiopoulos, W. Wernsdorfer, B. Moulton, M.J. Zaworotko, G. Christou, *J. Am. Chem. Soc.* 125 (2003) 15274.
- [15] C.M. Zaleski, E.C. Depperman, J.W. Kampf, M.L. Kirk, V.L. Pecoraro, *Angew. Chem., Int. Ed.* 43 (2004) 3912.
- [16] S. Osa, T. Kido, N. Matsumoto, N. Re, A. Pochaba, J. Mrozinski, *J. Am. Chem. Soc.* 126 (2004) 420.
- [17] M. Murugesu, M. Habrych, W. Wernsdorfer, K.A. Abboud, G. Christou, *J. Am. Chem. Soc.* 126 (2004) 4766.
- [18] M. Murugesu, W. Wernsdorfer, K.A. Abboud, G. Christou, *Polyhedron* (in press).
- [19] E.K. Brechin, J. Yoo, M. Nakano, J.C. Huffman, D.N. Hendrickson, G. Christou, *Chem. Commun.* (1999) 783.
- [20] C. Boskovic, W. Wernsdorfer, K. Folting, J.C. Huffman, D.N. Hendrickson, G. Christou, *Inorg. Chem.* 41 (2002) 5107.
- [21] M. Murugesu, W. Wernsdorfer, K.A. Abboud, G. Christou, *Angew. Chem.* 44 (2005) 792.
- [22] M. Murugesu, K.A. Abboud, G. Christou, *Dalton Trans.* (2003) 4552.
- [23] F.A. Hart, in: G. Wilkinson (Ed.), *Comprehensive Coordination Chemistry*, vol. 3, Pergamon, Oxford, 1987, p. 1073.
- [24] R.F. Weinland, A. Herz, *Ber. Deutsch. Chem. Ges.* 45 (1912) 2662.
- [25] M.W. Wemple, H.-L. Tsai, S. Wang, J.-P. Claude, W.E. Streib, J.C. Huffman, D.N. Hendrickson, G. Christou, *Inorg. Chem.* 35 (1996) 6450.
- [26] W. Wernsdorfer, *Adv. Chem. Phys.* 118 (2001) 99.
- [27] G.M. Sheldrick, *SHELXL-97*, Program for Refinement of Crystal Structures, University of Gottingen, Germany, 1997.
- [28] L. Wittick, K. Murray, B. Moubaraki, S. Batten, L. Spiccia, K. Berry, *Dalton Trans.* (2004) 1003.
- [29] M.A. Bolcar, S.M.J. Aubin, K. Folting, D.N. Hendrickson, G. Christou, *Chem. Commun.* (1997) 1485.
- [30] N.C. Harden, M.A. Bolcar, W. Wernsdorfer, K.A. Abboud, W.E. Streib, G. Christou, *Inorg. Chem.* 42 (2003) 7067.
- [31] C. Boskovic, E.K. Brechin, W.E. Streib, K. Folting, J.C. Bollinger, D.N. Hendrickson, G. Christou, *J. Am. Chem. Soc.* 124 (2002) 3725.
- [32] E.K. Brechin, M.J. Knapp, J.C. Huffmann, D.N. Hendrickson, G. Christou, *Inorg. Chim. Acta* 297 (2000) 389.
- [33] P. King, R. Clérac, W. Wernsdorfer, C.E. Anson, A.K. Powell, *Dalton Trans.* (2004) 2670.
- [34] C. Benelli, M. Murrie, S. Parsons, R.E.P. Winpenny, *Dalton Trans.* (1999) 4125.
- [35] J. Yoo, A. Yamaguchi, M. Nakano, J. Krzystek, W.E. Streib, L.-C. Brunel, H. Ishimoto, G. Christou, D. Hendrickson, *Inorg. Chem.* 40 (2001) 4604.
- [36] W. Wernsdorfer, N. Aliaga-Alcalde, D.N. Hendrickson, G. Christou, *Nature* 416 (2002) 406.